ISSN: 0067-2904

Analysis of Longitudinal Electroexcitation for Positive and Negative Parity States of ^{36,40}Ar Nuclei Using Different Model Spaces

A. A. Abdulhasan* ، Z. A. Dakhil
Department of Physics, College of Science, University of Baghdad, Baghdad, Iraq

Received: 30/9/2022 Accepted: 12/12/2022 Published: 30/10/2023

Abstract

The nuclear structure for the positive ($2^+_{1,2,3}$) States and negative (3^-_1) states of ^{36,40}Ar nuclei have been studied via electromagnetic transitions within the framework of shell model. The shell model analysis has been performed for the electromagnetic properties, in particular, the excitation energies, occupancies numbers, the transition strengths B(*CL*) and the elastic and inelastic electron scattering longitudinal form factors. Different model spaces with different appropriate interactions have been considered for all selected states. The deduced results for the (*CL*) longitudinal form factors and other properties have been discussed and compared with the available experimental data. The inclusion of the effective charges are essential for obtaining a reasonable description for the data. The results of sdpf-model space with *sdpfk* and *sdpfmu*-interactions have a good improved for the ground state form factors for ^{36,40}Ar and for excitation properties of 2^+_1 and 3^-_1 state of ^{36}Ar nucleus.

Keywords: Longitudinal form factor, Energy level, Transition strengths.

تحليل الاستثارة الالكترونية الطولية للحالات الموجبة والسالبة للنوى ^{36,40}Ar باستخدام أنموذج لفضاءات مختلفة

علي احمد عبدالحسن*، زاهدة احمد دخيل
قسم الفيزياء , كلية العلوم, جامعة بغداد, بغداد, العراق

الخلاصة

تم دراسة التركيب النووي للحالات الموجبة ($2^+_{1,2,3}$) والحالات السالبة (3^-_1) للنوى (^{36,40}Ar) عن طريق الانتقالات الكهرومغناطيسية ضمن حقل أنموذج القشرة. تم تقديم تحليل أنموذج القشرة للميزات الكهرومغناطيسية, خاصة, طاقة التحفيز
اعداد الاشغال, قوى الانتقال(*CL*)B وعوامل التشكل الطولية للاستطارة اللكترونية المرنة وغير المرنة. تم الاعتماد على فضاءات مختلفة مع تفاعلات مناسبة مختلفة لجميع الحالات المختارة.تم مناقشة النتائج المستحصلة لعوامل التشكل الطولية والمميزات الاخرى ومقارنتها مع المعطيات العملية المتوفرة. ادخال الشحنات الفعالة اساسي لوضع وصف مقبول للمعطيات العملية. نتائج الفضاء sdpf مع التفاعلات *sdpfk* و *sdpfmu* حسنت

*Email: ali.hamza1104@sc.uobaghdad.edu.iq

وبشكل جيد عوامل التشكل للحالة الارضية للنوى $^{36,40}Ar$ ولمميزات الحالات المحفزة (2_1^+) و (3_1^-) لنواة ^{36}Ar .

1. Introduction

High-energy electron - nucleus scattering is precise tool for probing nuclear structure. The theoretical description of the electron scattering is challenging due to the significant influence of the nuclear electromagnetic properties. With the rapid development of the experiments great efforts have been devoted to the theoretical studies of the electron scattering of nuclei in the last decade **[**1-5].

The interest for exotic nuclei has increased enormously since the recent progress in nuclear accelerators. It is important and interesting to explore the properties of exotic nuclei both theory and experiment. Most of the nuclei are found to be deformed in their ground states [6, 7, 8]. The present study sheds some light not only on the structured positive parity states ($J^\pi = 2_L^+$) of ^{36}Ar and ^{40}Ar isotopes, but also on the available negative parity states which denoted by ($J^\pi = 3_1^-$) and restricted to low energy of a few *Mev*. The electromagnetic properties of first excited 2_L^+ states are primarily considered of both ^{36}Ar and ^{40}Ar isotopes. The ^{36}Ar ($N = Z = 18$) nucleus has several interesting features therefore, it has attracted considerable experimental and theoretical investigations. The measurements of the g-factors, Lifetimes and the transition probabilities B (*E2*) of the 2_L^+ states in ^{36,38,40}Ar are performed by Speidel et al. [9], and explained by Large - scale shell model calculations. Recently, Riczu and Cseh. [10] reported gross features of the spectrum of ^{36}Ar nucleus. Their calculations are included the superderfomed and the hyperdeformed States In addition to the ground state region. They applied the multiconfigurational dynamical symmetry (Musy) reproduce these gross feature of the spectrum. The Musy is denoted to the connection between the deformation, clusterization and shell structure in terms of a dynamical symmetry [11].

In the present work, three different model spaces have been used for the positive - parity 2_L^+ states of ^{36}Ar. The first is sdpf-model space with *sdpfk*-interaction in which ^{36}Ar is considered as ^{16}O ($N = Z = 8$) inert core with active sd and fp-shell's. The second one is Hasp-model space with the *hasn*-interaction here four active protons and neutrons are covered the active shells $2s_{1/2}$, $1d_{3/2}$, $1f_{7/2}$ and $2p_{3/2}$ .The last one is the sd-shell model space with new USD - type interaction Viz the *usdi*-interaction [12]. This interaction improved the predictions for separation energy in the entire sd-shell. Together with these interactions, we have been also used the sdpf - model space with the *sdpfk* and *sdpfum*-interactions for positive parity 2_L^+ states of ^{40}Ar, which comprise the active sd and fp-shell's above the inert core ^{16}O nucleus. For negative parity states of ^{36}Ar and ^{40}Ar nuclei, the d3f7, hasp and sdpf-model spaces with *Wo*, *hasn* and *sdpfmu*-interactions have been used respectively [13, 14, 1]. The first model space (d3f7) with *Wo*-interaction for ^{36}Ar and ^{40}Ar are considered as ^{32}S ($N = Z = 16$) inert core with two active protons and neutrons for ^{36}Ar and four active protons and neutrons for ^{40}Ar, distributed among active shells $1d_{3/2}$ and $1f_{7/2}$. The excitation energies, occupancies and B(*C2*) transition strengths are calculated . This work is extended to study the various CL Components longitudinal electron scattering form factors. The present calculations are performed using shell model OXBASH code [15]. The shell model within the restricted model space is not enough to describe the electric properties. The core polarization effects are introduced through different effective charges. Bohr - Mottelson (*B-M*) effective charges [16], and standard (*ST*) proton and neutron effective charges ($e_p^{eff} = 1.36\, e$, $e_n^{eff} = 0.45\, e$) [17] are adopted.

2. Theoretical Formalism

The differential cross section in the plane - wave Born approximation (PWBA) for the scattering of electron with initial total energy E_i and final total energy E_f from a nucleus of mass M and charge Ze through an angle (Θ) is given by [18, 19];

$$\frac{d\sigma}{d\Omega} = \sigma_{Mott}\ \eta \sum_{L} \left| F\left(L,q\right) \right|^2 \tag{1}$$

The Mott cross section σ_{Mott} for relativistic electron scattering from a massive point charge is given by;

$$\sigma_{Mott} = Z^2 \alpha^2 \cos^2\left(\theta/2\right) / 4E_i^{\,2} \sin^4\left(\theta/2\right) \tag{2}$$

Where $\alpha = e^2/\hbar c$ is the fine-structure constant. The target-recoil factor η is given by;

$$\eta = [1+(2E_i/M)\sin^2(\theta/2)]^{-1} \tag{3}$$

The longitudinal form factor $F_L^{C}(q)$ of a given multipolarity (L), as a function of momentum transfer (q) between initial (J_i) and final (J_f) nuclear states can be written in terms of Many-nucleon matrix elements reduced in both angular momentum (J) and isospin (T) as follows [20];

$$\left|F_L^{C}(q)\right|^2 = \frac{1}{(2J_i+1)}\left(\frac{4\pi}{Z^2}\right)\left|\sum_{T=0,1}(1-)^{T_f-T_{zf}}\begin{pmatrix} T_f & T & T_i \\ -T_{zf} & M_T & T_{zi}\end{pmatrix}\left\langle f \left\| L_{LT}^{Coul}(q) \right\| i \right\rangle F_{cm}(q) F_{fs}(q)\right|^2 \tag{4}$$

The normalization ($4\pi/Z^2$) ensures that the longitudinal elastic scattering form factor equates to unity at zero momentum transfer $T_z=(Z-N)/2$. $L_{LT}^{Coul}(q)$ is the longitudinal multipole operator, L is determined from the parity selection rules, the bracket $\begin{pmatrix} \cdot & \cdot & \cdot \\ \cdot & \cdot & \cdot \end{pmatrix}$ denotes the *3j*-symbols. The center of mass correction is $F_{c.m.} = e^{q^2b^2/4A}$ [21] is the correction for the lack of translation invariance in the shell model and the nucleon finite size ($F_{f.s.}$) form factor is [22], $F_{f.s.}(q) = [1+(q/4.33)^2]^{-2}$. The Many- nucleon reduced matrix element of L_L^{Coul} operator can be written as the sum of the product of the one-body density matrix (OBDM) times the reduced single- particle matrix elements [23];

$$\left\langle f \left\| L_L^{Coul}(q) \right\| i \right\rangle = \sum_{j,j'} OBDM\ \ (L,j,j',f,i,t_z)\left\langle j \left\| L_L^{Coul}(q,t_z) \right\| j' \right\rangle \tag{5}$$

For elastic longitudinal electron scattering, the sum includes the core level, for inelastic scattering, the sum extends across all pairs of single-particle states j, j' (isospin is included).

The reduced single particle matrix elements used in the present work are those of Brown et al. [24].

The (OBDM) in spin-isospin formalism are obtained in the form [25];

$$OBDM\ (J_f,J_i,j,j',,L,t_z) = (-1)^{T_f-T_z}\begin{pmatrix} T_f & 0 & T_i \\ -T_Z & 0 & T_Z\end{pmatrix}\sqrt{2}\frac{OBDM\ (\Delta T=0)}{2}$$

$$+2t_z(-1)^{T_f-T_z}\begin{pmatrix} T_f & 1 & T_i \\ -T_Z & 0 & T_Z\end{pmatrix}\sqrt{6}\frac{OBDM\ (\Delta T=1)}{2} \tag{6}$$

In the second quantization formalism, the OBDM takes the form,

$$OBDM\ (J_i,J_f,j,j',L,\Delta T) = \frac{\left\langle f \left\| \left[a_{(j)}^{+}\otimes \tilde{a}_{(j')}\right]^{(L,\Delta T)} \right\| i \right\rangle}{\sqrt{2L+1}\sqrt{2\Delta T+1}} \tag{7}$$

The form factor is related to the reduced transition probability at the photon point as [24];

$$B(EL) = \frac{[(2L+1)!!]^2 Z^2 e^2}{4\pi k^{2L}} \left| F_L^{Coul}(q=k) \right|^2 \quad (8)$$

where $K = E_x / \hbar c$, B(*EL*) is in unit of $e^2 fm^{2L}$.

3. Results and Discussion

The nuclear structure properties for positive – negative parity states of ^{36}Ar, and ^{40}Ar nuclei have been studied. The nuclear shell model Calculations are restricted to low - energy states of few *Mev* for $0_1^+ \to 2_L^+$ and $0_1^+ \to 3_1^-$, transitions (with L = 1,2,3). The single particle harmonic oscillator (HO) Potential with size parameter (b) is used to generate the single - particle wave functions. The oscillator length (b) is obtained from [25];

$$b = \sqrt{\frac{\hbar}{M_p W}} \quad \text{with} \quad \hbar w = 45A^{-1/3} - 25A^{-2/3} \quad (9)$$

All calculations are carried out using the OXBASH code [15] for different model spaces with an appropriate interactions. The SD, HASP, D3F7 and SDPF model spaces are used with the *usdi, hasn, Wo, sdpfk* and *sdpfmu* interactions, respectively. The calculations with only model space wave functions are inadequate for reproducing the electron scattering data [26]. Therefore, the contributions of the higher configurations outside the model space are essential to improve the predicted results. The core polarization effects are included through two different proton and neutron effective charges. Bohr – Mottelson (*B-M*) [16] formulated the following expression for effective charges,

$$e_{eff}(t_z) = e(t_z) + e\delta e(t_z)$$
$$\delta e(t_z) = \frac{Z}{A} - 0.32\frac{(N-Z)}{A} - 2t_z[0.32 - 0.3\frac{(N-Z)}{A}] \quad (10)$$

Also, the standard (*ST*) proton and neutron effective charges ($e_p^{eff} = 1.36\, e$, $e_n^{eff} = 0.45\, e$) [17].

Discussion of the present results will be divided into two parts; The first one pertains to elastic longitudinal electron scattering and the second one is related to inelastic longitudinal electron scattering. Both parts include, the longitudinal electron scattering form factors, excitation energies, transition strengths B(*CL*).

3.1. Elastic Longitudinal Electron Scattering Form Factors (J^π=0)

The *Co* longitudinal form factors for ^{36}Ar nucleus are calculated using model spaces with three different interactions and shown in Figure (1-a), *usdi*-interaction (green curve), *hasn*-interaction (purple curve) and *sdpfmu*-interaction (blue curve). For ^{40}Ar nucleus, the Co form factors are calculated using, full SDPF model space with the *sdpfmu*-interaction (blue curve) and *sdpfk*-interaction (black curve) as shown in Figure (1-b). The experimental data (red full circle) [26], are covering the range of momentum transfer ($0.539 \le q \le 0.96$) fm^{-1}. The Co form factor is clearly dominated at low q-region, with further diffraction structures at $q > 1.0$ fm^{-1}. The diffraction minima are located at the same region of *q* for both interactions in ^{40}Ar, with some deviation in the second minimum of *hasn*-interaction for both ^{36}Ar and ^{40}Ar nuclei an overall agreement is obtained for all interactions through all the experimental q-regions.

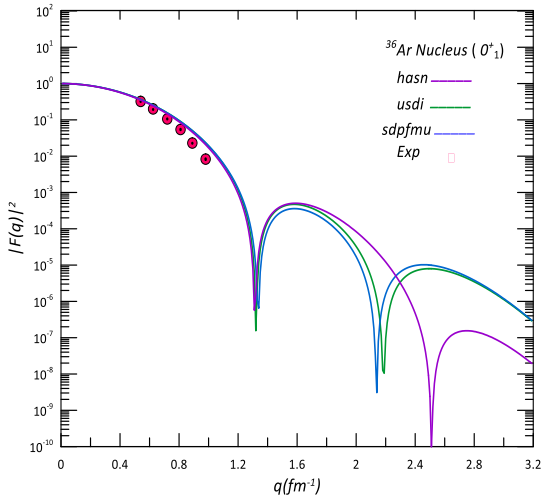

Figure (1-a): Elastic longitudinal form factor for 0^+ state in ^{36}Ar compared with experimental data of Ref. [26].

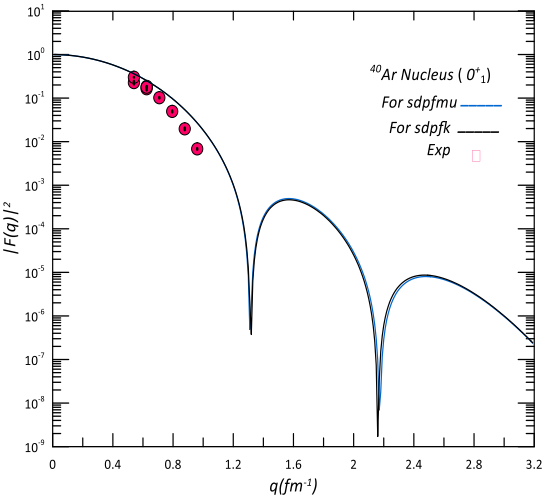

Figure (1-b): Elastic longitudinal form factor for 0^+ state in ^{40}Ar compared with experimental data of Ref. [26].

3.2. Inelastic Longitudinal Electron Scattering Form Factors ($J^\pi = 2^+_L$)

The main focus of the discussion will be on the transitions ($0^+_1 \rightarrow 2^+_L$) and ($0^+_1 \rightarrow 3^-_1$) with the levels ($L = 1, 2, 3$). For (2^+_1) excited state of ^{36}Ar nucleus the occupancies of ($1d_{5/2}$,$2s_{1/2}$, $1d_{3/2}$), ($1d_{3/2}$, $2s_{1/2}$, $1f_{7/2}$, $2p_{3/2}$), and ($1d_{5/2}$, $2s_{1/2}$, $1d_{3/2}$, $1f_{7/2}$, $2p_{3/2}$, $1f_{5/2}$, $2p_{1/2}$) proton and neutron orbitals with *usdi*, *hasn and sdpfk*-interactions, respectivly, are shown in Figure(2-a) with configurations [$(1s)^4(1p)^{12}$], [$(1s)^4(1p)^{12}(1d_{5/2})^{12}$] , and [$(1s)^4(1p)^{12}$] inert core respectivly. In general view, both *usdi* and *sdpfk*-interactions are giving the highest percentage configuration mixture with 95.9% ($1d_{5/2}$) orbit, while , the *hasn*-interaction appeared lower percentage with 54 % ($1d_{3/2}$) orbit. For the negative parity state (3^-_1) of ^{36}Ar, the occupancies of ($1d_{3/2}$, $1f_{7/2}$), ($1d_{3/2}$, $2s_{1/2}$, $1f_{7/2}$, $2p_{3/2}$), and full sdpf model space proton and neutron orbitals with *Wo*, *hasn and sdpfmu*-interactions, respectivly, are shown in Figure(2-b). The contribution of proton and neutron occupancy is dominant from $1d_{5/2}$ for *SDPF*-model space with *sdpfmu*-interaction. . A lower percentage configuration mixture appeared in this state with 35% and 54% ($1d_{3/2}$) orbit for *Wo* and *hasn*-interactions respectively. The positive parity state (2^+_1) of ^{40}Ar has the configuration of [$(1s)^4(1p)^{12}$] inert core . The occupancies of ($1d_{5/2}$, $2s_{1/2}$, $1d_{3/2}$, $1f_{7/2}$, $2p_{3/2}$, $1f_{5/2}$ and $2p_{1/2}$) proton and neutron orbitals with *sdpfk* and *sdpfmu*-interactions are shown Figure (2-c). The dominant contribution of neutron occupancy is appeared from ($1d_{5/2}$) orbit for both *sdpfk* and *sdpfmu*-interactions, with percentage configuration mixture of 99.4 %. The negative parity state (3^-_1) of ^{40}Ar has the same configurations and interactions of that of ^{36}Ar and is shown in Figure (2-d). The contribution of neutron occupancy for both *Wo* and *hasn* interactions is smaller in Comparison to that of ($1d_{5/2}$) orbit for *sdpfmu*-interaction. In general, the ($1d_{5/2}$) orbital has important and significant role of occupation numbers in the sd - model space (with ($(1s)^4(1p)^{12}$ inert core) for both ^{36}Ar and ^{40}Ar. The role of ($1d_{5/2}$) orbital is important as the neutron number is increased as well as other sd-shell nuclei [27].

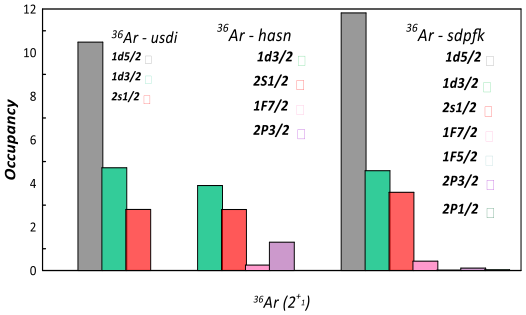

Figure (2-a): Bar chart of the occupancies for ^{36}Ar (2_1^+) with *usdi*, *hasn* and *sdpfk*-interactions.

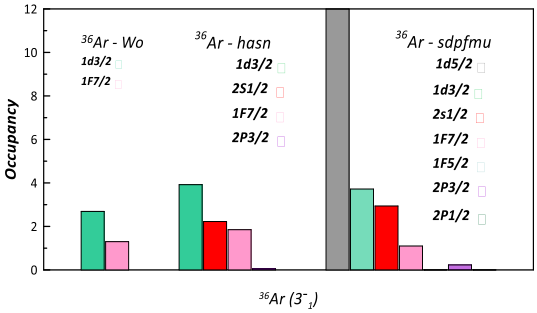

Figure (2-b): Bar chart of the occupancies for ^{36}Ar (3_1^-) with *Wo*, *hasn* and *sdpfmu*-interactions.

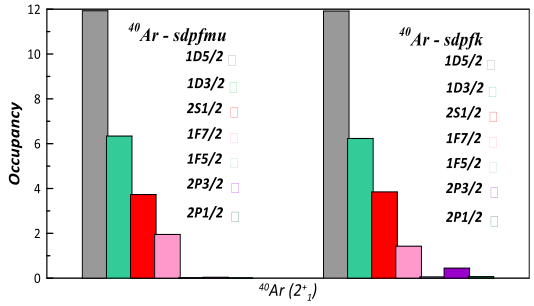

Figure (2-c): Bar chart of the occupancies for ^{40}Ar (2_1^+) with *sdpfk and sdpfmu*-interactions.

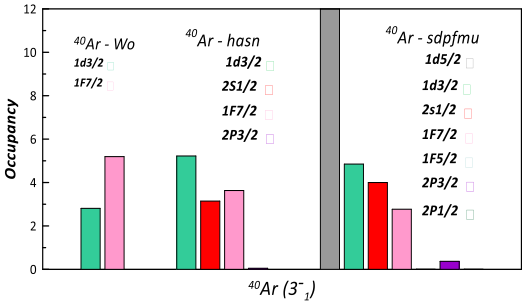

Figure (2-d): Bar chart of the occupancies for ^{40}Ar (3_1^-) with *Wo*, *hasn* and *sdpfmu*-interactions.

The excitation energies of these states are calculated with the *usdi*, *hasn*, *sdpfk*-interactions for ^{36}Ar nucleus, also with *sdpfk* and *sdpfmu*-interactions for ^{40}Ar nucleus, and displayed in Figure (3). The calculated energies are listed in Table (1) together with the measured values [26, 28], and other results for comparison. For ^{36}Ar, the results of 2_1^+ state with *usdi*, *hasn*, *sdpfk*-interactions (1.818*MeV*, 1.82*MeV* and 1.766*MeV* respectively), provide a good agreement with both measure value (1.97±0.05*MeV*) and that of Ref. [3] as well as for other 2_2^+ and 2_3^+ levels. For ^{40}Ar, the results with *sdpfk*-interaction for $2_1^+, 2_2^+$, and 2_3^+ levels (1.546*MeV*, 3.06*MeV* and 3.887*MeV* respectively), reproduced the measured values (1.46±0.05*MeV*, 2.524±0.01*MeV* and 3.207 ± 0.013*MeV* respectively) and slightly better than that of *sdpfu*-interaction. The result of *sdpfmu*-interaction (1.028*MeV*) for the first level is underestimated compared with the measured value (1.46±0.05*MeV*) and with that of Ref. [3] (1.28*MeV*). The excitation energies for the negative parity state (3_1^-) of both ^{36}Ar and ^{40}Ar nuclei are calculated with *Wo*, *hasn* and *sdpfmu*-interactions. The results of *Wo*-interaction are the best for both ^{36}Ar and ^{40}Ar (4.797*MeV* and 4.018*MeV* respectively) in comparison with the measured values (4.178±0.01*MeV* and 3.680±0.012*MeV*), but becomes significantly worse for *sdpfmu*-interactions for both ^{36}Ar and ^{40}Ar (8.0*MeV* and 7.5*MeV* respectively). The results of *sdpfmu*-interaction over-predict the data by about a factor of two.

Table 1: The excitation energies (*MeV*) for positive & negative-parity states in ^{36}Ar and ^{40}Ar for different model space, compared with experimental data of Refs. [26, 28];

Nucleus	J_L^π	$Ex_{exp.}$ (*MeV*)	$Ex_{cal.}$		
			USDI	***HASN***	***SDPFK***
^{36}Ar	2_1^+	1.97±0.05	1.818	1.82	1.766
	2_2^+	4.440±0.019	4.20	4.15	3.4
	2_3^+	4.951±0.04	6.0	4.61	4.24
			SDPFK		***SDPFMU***
^{40}Ar	2_1^+	1.460±0.05	1.546		1.028
	2_2^+	2.524±0.011	3.061		3.168
	2_3^+	3.207±0.013	3.887		2.499

Nucleus	J_n^π	$Ex_{exp.}$ (*MeV*)	$Ex_{cal.}$		
			W0	***HASN***	***SDPFMU***
^{36}Ar	3_1^-	4.178±0.011	4.797	3.443	8.0
^{40}Ar	3_1^-	3.680±0.012	4.018	2.693	7.5

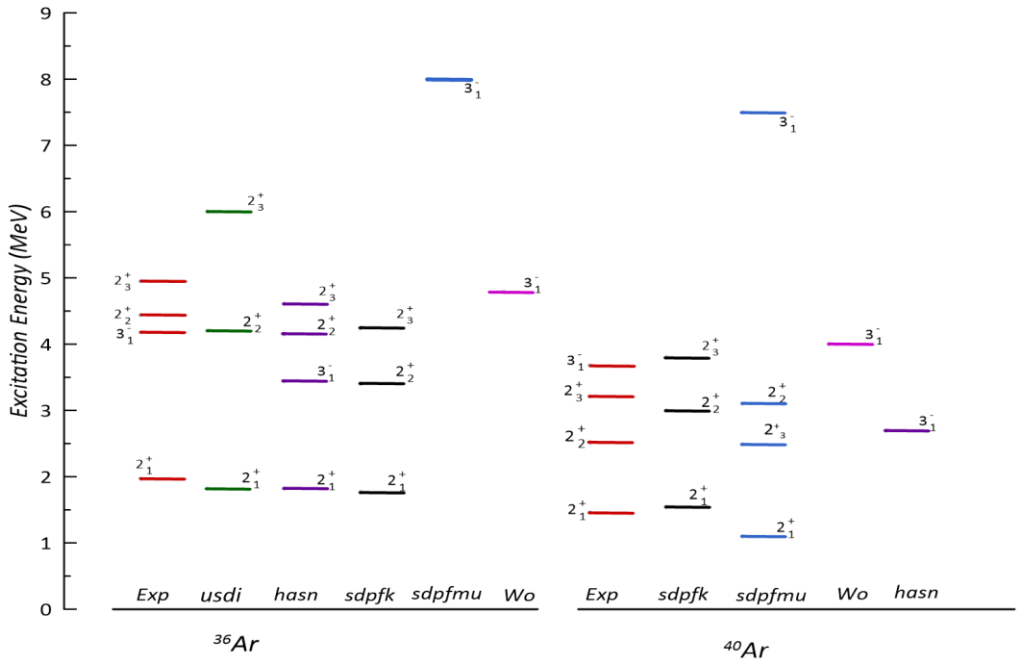

Figure 3: Low-lying energy spectra for ^{36,40}Ar. Theoretical shell model results with different interactions for change parity states are compared with experimental data of Refs. [26, 28]**.**

3.2.1. The Inelastic C2 Form Factor for Positive Parity states ($J^\pi = 2_L^+$)

The inelastic longitudinal form factors are calculated using different model spaces with different interactions, as mentioned previously. The results of each interaction with *B-M* effective charges, are denoted by solid curve, and the dashed curve for the results with the standard effective charges ($e_p^{eff} = 1.36\, e$, $e_n^{eff} = 0.45\, e$), while the dashed-dot curve represents the results of model space only. For ^{36}Ar, the longitudinal *C2* form factors for 2_1^+ state with *B-M* ($e_p^{eff} = 1.18, e_n^{eff} = 0.82$) and *ST* effective charges are displayed in Figure (4-a). The results

with both *sdpfk* and *hasn*-interactions (black and purple curves respectively) explain the C2 data [26] very well over all regions of momentum transfer. The C2 form factors for the *usdi*-interaction with both effective charges (green curves) are over predict the q-data. The predicted transition strength with *usdi*-interaction (B(*C2*) = 323.2 e^2fm^4) is very close to both measured value [26] (B (*C2*) = 301($^{+20}_{-11}$) e^2fm^4) and to that of Ref [3]. The results of *sdpfk* and *hasn* interactions (259 e^2fm^4 and 274.6 e^2fm^4 respectively) are also in a good agreement with measured value within the experimental error as shown in Table (2).

The longitudinal *C2* form factors for 2^+_2 and 2^+_3 states for all three interactions with both *B-M* and *ST* effective charges are shown in Figure (4-b) and Figure (4-c), respectively. There is no available experimental data for these states. The results of *usdi* and *hasn*-interactions with *B-M* for 2^+_2 state are close to each other in the range of $0.1<q<1.8$ fm^{-1}, with two diffraction minima of *hasn*-interaction, while the first diffraction minima are coincidentally located at $q \approx 1.1$ fm^{-1}. The same result and behavior can be noticed for 2^+_3 state for *sdpfk* and *hasn*-interactions with *B-M* effective charges. It is obvious that the result of *sdpfk*-interaction shows different behavior with a clear discrepancy compared from that of both *usdi* and *hasn*-interactions. No diffraction minima appeared with *sdpfk* interaction for 2^+_2 state and appeared at $q \approx 1.3$ fm^{-1} for 2^+_3 state.

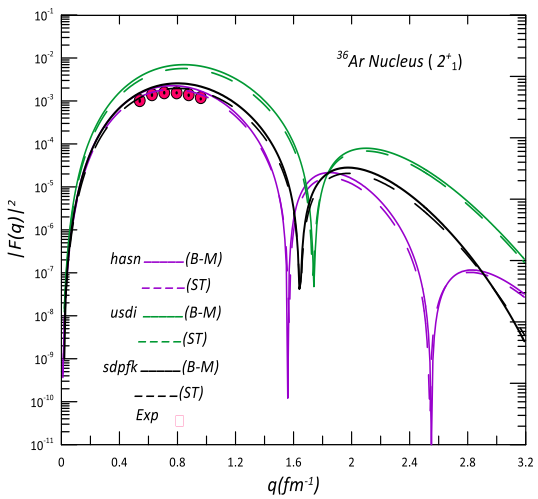

Figure (4-a): Inelastic longitudinal *C2* form factor for 2^+_1 state in ^{36}Ar nucleus, compared with experimental data of Ref [26].

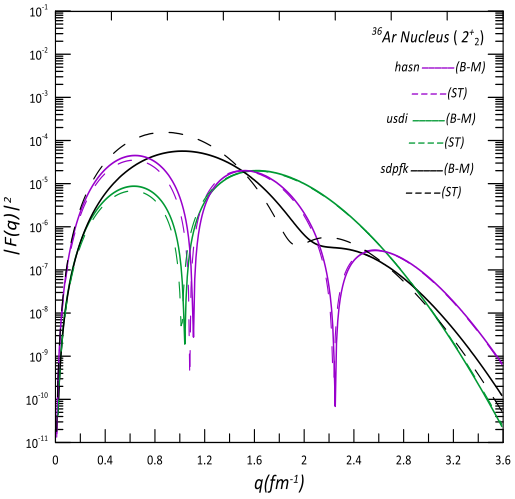

Figure (4-b): Inelastic longitudinal *C2* form factor for 2^+_2 state in ^{36}Ar nucleus.

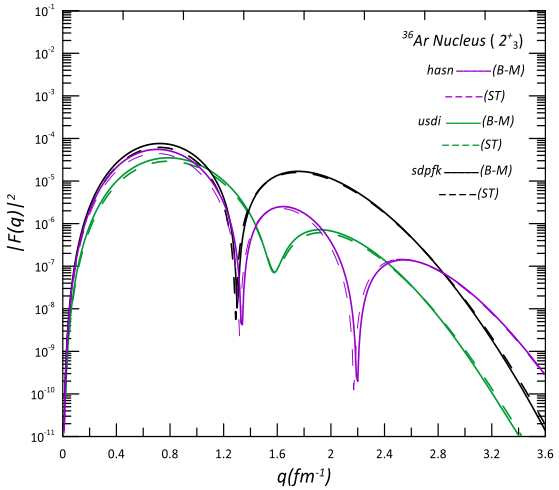

Figure (4-c): Inelastic longitudinal C2 form factor for 2_3^+ state in ^{36}Ar nucleus.

For ^{40}Ar, the inelastic longitudinal C2 form factors for 2_L^+ states are calculated using full sdpf model space with *sdpfk* and *sdpfmu*-interactions. The results with effective charges ($e_p^{eff}=1.128, e_n^{eff}=0.708$) of *B-M* and ($e_p^{eff}=1.36\,e$, $e_n^{eff}=0.45\,e$) standard values are compared together with that of bare nucleon charges as well as with the available experimental data [26]. The predicted *C2* form factor for 2_1^+ state is compared with available experimental data [26] and depicted in Figure (5-a). In spection of these curves reveals that the results of *sdpfk* and *sdpfmu*-interactions with bare nucleon charges (dashed-dot curves) exhibit qualitative similarity to the shape of the experimental data and underestimate in its magnitude. The core polarization effects with standard effective charges (dashed curves) for both interactions give a good description of the experimental data and slightly overestimate the data with *B-M* effective charges at $q \approx 1.0$ fm^{-1}. The predicted B(*C2*) for 2_1^+ state with *sdpfk*-interaction (299.7 e^2fm^4) and with sdpfmu-interaction (223.9 e^2fm^4) have well improved the description of the measured B(*C2*) of Ref.[29] (332±17e^2fm^4) within the experimental error. The *sdpfmu*-result is close to that of Ref [3] (245 e^2fm^4) as shown in Table (2). The longitudinal C2 fare factors for 2_2^+ state for both *sdpfk* and *sdpfmu*-interactions are compared with available experimental data [26] and displayed in Figure (5-b). It is clear that the results of *ST* effective charges (dashed curves) are close to that of bare nucleon charges (dashed-dot curves) for both interactions, and overestimate state the experimental dada at $q > 0.6$ fm^{-1}. The predicted *C2* form factors with *B-M* effective charges for both interactions are in a reasonable agreement with the experimental data. The measured transition strength B(*C2*) (45+24 e^2fm^4) [26], is well reproduced with both *sdpfk* and *sdpfmu*-interactions (30.2 and 31.7 e^2fm^4 respectively).

The inelastic *C2* form factors for 2_3^+ state with *sdpfk* and *sdpfmu*-interaction are shown in Figure (5-c). The *sdpfmu*-interaction with bare nucleon charges (dashed-dot curves) gives a remarkable agreement with the available experimental data [26], and slightly overestimate the data with *B-M* effective charges. The *C2* form factors for *sdpfk*-interaction with bare and effective charges are broadly consistent with the major trends of the experimental data. This behavior is clearly appeared in the predicted B(*C2*) strengths as shown in Table (2).

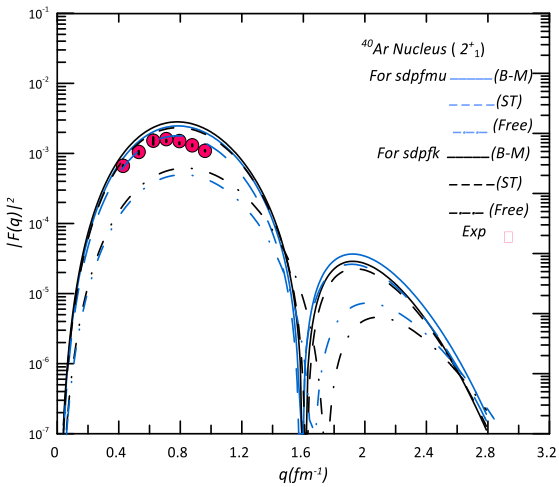

Figure (5-a): Inelastic longitudinal C2 form factor for 2^+_1 state in ^{40}Ar nucleus.

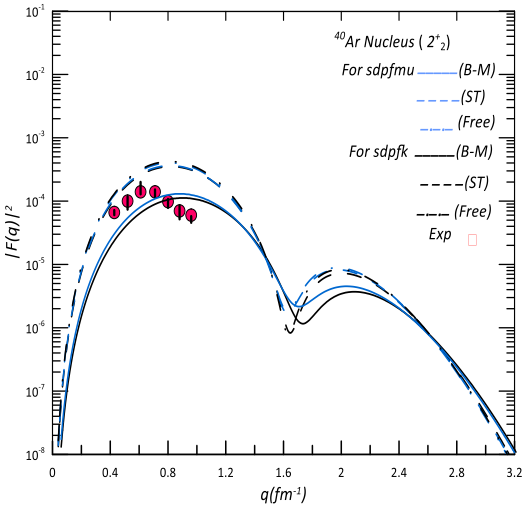

Figure (5-b): Inelastic longitudinal C2 form factor for 2^+_2 state in ^{40}Ar nucleus.

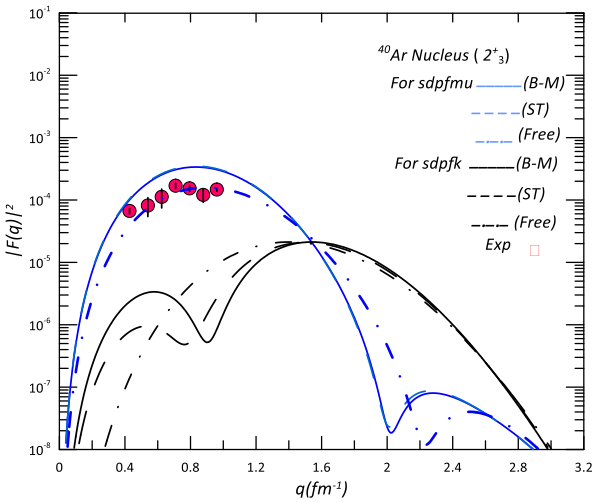

Figure (5-c): Inelastic longitudinal C2 form factor for 2^+_3 state in ^{40}Ar nucleus.

3.2.2. The Inelastic Longitudinal Form Factors for Negative Parity state ($J^\pi = 3^-_1$)

The Longitudinal *C3* form factors for 3^-_1 stare at 4.178*MeV* of ^{36}Ar and at 3.680*MeV* of ^{40}Ar are calculated using D3F7, HASP and SDPF-model spaces with *Wo*, *hasn* and *sdpfmu*-interactions. The comparison with available experimental data are shown in Figure (6-a) and Figure (6-b) for ^{36}Ar and ^{40}Ar respectively. For ^{36}Ar, the predicted *C3* form factors with bare and effective charges for all interactions are displayed in Figure (6-a). In the light of the best agreement with the experimental data is due to the extended SDPF and HASP model spaces (blue and purple Curves). The results of *sdpfmu* and *hasn* interactions reproduce more precisely the experimental data over all *q*-regions. The longitudinal *C3* form factor of *Wo*-interaction has the same behavior in the shape for that of other interactions and underestimated in magnitude. The predicted B(*C3*) strengths for *sdpfmu* and *hasn*-interactions (0.76E+4 and 0.614E+4 e^2fm^6 respectively) are underestimated by about a factor of 2. While that of *Wo*-interaction is far away from the measured value of B(*C3*) [26] (1.62±0.2)E+4 e^2fm^6). For ^{40}Ar, the Longitudinal *C3* form factors for 3^-_1 state at 3.68*MeV* with *Wo*, *hasn* and *sdpfmu* interactions are compared

with available experimental date and illustrated in Figure (6-b). It is obvious that all these curves have almost the same shape and different in magnitude.

The *hasn* interaction yield an adequate description of the experimental data and better than that of other interactions which they a slight deviation below the experimental dada. The predicted B(*C3*) strength (0.3E+4 e^2fm^6) is underestimated by about a factor of 3 for *hasn*-interaction and more than this for other interaction as listed in Table (2).

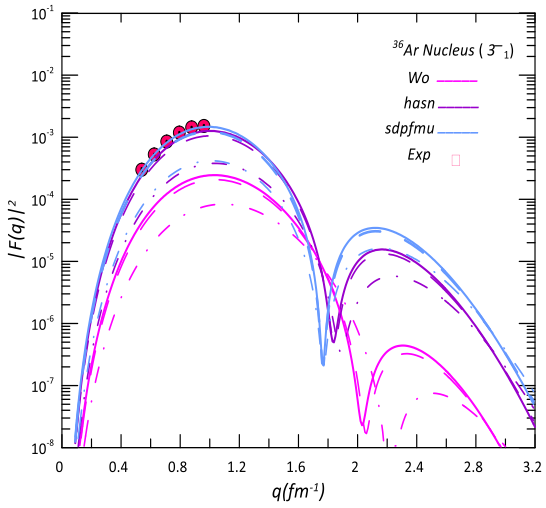

Figure (6-a): Inelastic longitudinal C3 form factor for 3^-_1 state in ^{36}Ar nucleus.

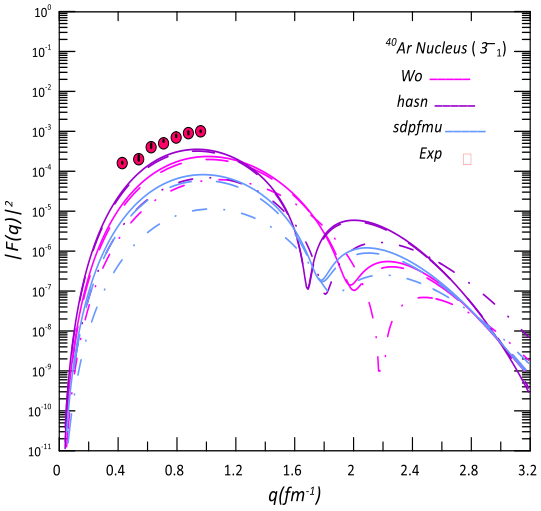

Figure (6-b): Inelastic longitudinal C3 form factor for 3^-_1 state in ^{40}Ar nucleus.

Table 2: The reduced transition probability (B(CL)e^2fm^{2L}) for positive and negative-parity states in ^{36}Ar and ^{40}Ar for different model space compared with the experimental data of Refs. [26, 28]; (a): [3], (b): [9]

Nucleus	J^π_n	$B(CL)_{exp.}$ (e^2fm^{2L})	$B(CL)_{cal.}$			
			SDPFK	***HASN***	***USDI***	***Other St.***
^{36}Ar	2^+_1	$301(^{+20}_{-11})$	259	274.6	323.2	324 [a] 322 [b]
	2^+_2	(-)	1.64	9.42	2.0	
	2^+_3	3 [a]	10.1	8.4	3.5	
			SDPFK		***SDPFMU***	
^{40}Ar	2^+_1	332±17	299.7		223.9	245 [a] 241 *DOI: 10.24996/ijs.2023.64.10.43* [b]
	2^+_2	45±24	30.2		31.71	
	2^+_3	29±17	0.976		28.8	

Nucleus	J^π_n	$B(CL)_{exp.}$ (e^2fm^{2L})	$B(CL)_{cal.}$		
			W0	***HASN***	***SDPFMU***
^{36}Ar	3^-_1	(1.62±0.2)E+4	0.12E+4	0.614E+4	0.76E+4
^{40}Ar	3^-_1	(1.08±0.2)E+4	0.113E+4	0.3E+4	0.015E+4

4. Conclusions

In the present work, different model spaces with different interactions have been used to investigate the nuclear structure of positive ($2^{+}_{1,2,3}$) states and negative (3^{-}_{1}) parity states of ^{36,40}Ar nuclei. The contribution nucleon occupancy is dominant from ($1d_{5/2}$) orbit. The SDPF model space has a remarkable improvement in both shape and magnitude for elastic and inelastic longitudinal form factors for positive ($2^{+}_{1,3}$) and negative (3^{-}_{1}) states, while is broadly consistent with the major trends of the experimental data for positive (2^{+}_{2}) state. The inclusion of the effective charges are adequate to obtain a reasonable agreement between the predicted results and the experimental data. The discrepancies in excitation energies (*Ex*) and transition strengths B(*C3*) with *sdpfmu*-interaction are clearly appeared, with good agreement for ($2^{+}_{1,2,3}$) positive parity states. Extending the model space to include higher energy configuration explains the C2 form factor data remarkably well.

References

[1] K. Kaneko, Y. Sun, T. Mizusaki, and M. Hasegawa;" Shell-model study for neutron-rich sd-shell nuclei" *Phys. Rev. C* 83, 014320, pp.1101-1571, 2011.

[2] R. A. Radhi, Z. A. Dakhil and N. S. Manie;" Microscopic calculations of quadrupole moments in Li and B isotopes" *Eur. Phys. J. A,* vol. 50: 115, 14115, pp.1-9, 2014.

[3] R. A. Radhi, A. H. Ali " Microscopic calculations of effective charges and quadrupole transition rates in Si, S and Ar isotopes" *Iraqi Journal of Science*, vol. 57, Issue 3B, pp.1999-2013, 2016.

[4] U. Gayer, T. Beck, M. Bhike, J. Isaak, N. Pietralla, P. C. Ries, D. Savran, M. Schilling, W. Tornow, and V. Werner " Experimental M1 response of 40Ar as a benchmark for neutrino-nucleus scattering calculations" *Phys. Rev. C* 100, 034305, pp.1-17, 2019.

[5] Sh. k. Raheem and Z.A. Dukhil, Acceptation *Iraqi Journal of science*, to be published in vol.63, Issue 12, 2022.

[6] N.J. Stone "Table of Nuclear electric quadrupole moments" *Atomic Data and Nuclear Data Tables,* 111-112, pp1-28, 2016.

[7] B. Longfellow, D. Weisshaar , A. Gade, B. A. Brown, D. Bazin , K. W. Brown, B. Elman, J. Pereira, D. Rhodes and M. Spieker;" Quadrupole collectivity in the neutron-rich sulfur isotopes ^{38,40,42,44}S" *Phys. Rev. C*, 103, 054309-15, 2021.

[8] Priyanka Choudhary and Praveen C. Srivastava," Ab initio description of Si, P, S, Cl and Ar isotopes in sd-shell" arXiv: 2204.00918, Vol.1 [nucl-th], 2022.

[9] K.-H. Speidel, S. Schielke, J. Leske, J. Gerber, P. Maier-Komor, S.J.Q. Robinson, Y.Y. Sharon, L. Zamick," Experimental g factors and B(E2) values in Ar isotopes: Crossing the N = 20 semi-magic divide" *Physics Letters B,* 632, pp. 207–211, 2006.

[10] Gábor Riczu and József Cseh" Gross features of the spectrum of the 36 Ar nucleus" *International Journal of Modern Physics E*, vol. 30, No. 05, 2150034, 2021.

[11] J. Cseh," Shape isomers and their clusterization" *Journal of Phys. Conf. Ser*. 580 -012057, 2015.

[12] A. Magilligan and B. A. Brown," New isospin-breaking “USD” Hamiltonians for the sd shell" *Phys. Rev. C* 101, 064312, 2020.

[13] K. K. Seth, A. Saha, W. Benenson, W. A. Lanford, H. Nann, and B. H. Wildenthal " Discovery of the Missing Two-Particle, Two-Hole 0+ States in 40Ca" Phys. Rev. Lett., vol.33, pp.233-236, 1974.

[14] H. Hasper " Large scale shell-model calculations in the upper part of the sd shell: General description and energy levels for A=36−39 " *Phys. Rev. C* ,19, pp.1482-1497, 1979.

[15] B. A. Brown, A. Etchgoyen, N. S. Godwin, W. D. M. Rae,W. A. Richter, W. E. Ormand, E. K. Warburton, J. S. Winfield, L. Zhao and C. H. Zimmerman, MSU-NSCL report Number 1289, 2005.

[16] A. Bohr, B. R. Mottelson "*Nuclear Structure", Benjamin, New York,* 2, 1975.

[17] W. A. Richter, S. Mkhize, and B. A. Brown "sd-shell observables for the USDA and USDB Hamiltonians" *Phys. Rev. C* 78. 064302, pp.1-7 2008.

[18] T. De Forest and J.D. Walecka "Electron Scattering and Nuclear Structure" *Adv . Phys*., vol. 15, Issue 57, pp. 100-109, 1966.
[19] T.W - Donnely and J. D. Walecka "Electron Scattering and Nuclear Structure" *Nucl . Phys*. A201, p.81, 1973.
[20] T.W. Donnelly and I. Sick "Elastic magnetic electron scattering from nuclei" *Reviews of Modern Physics*, vol. 56, no. 3, pp. 461-566, 1984.
[21] J. Tassie and F. C. Barker " Application to Electron Scattering of Center-of-Mass Effects in the Nuclear Shell Model" *Phys. Rev*. 111, 940, 1958.
[22] P. Glickman, W. Bertozzi, T. N. Buti, S. Dixit, F. W. Hersman, C. E. Hyde- Wright, M. V. Hynes, R. W. Lourie, B. E. Norum, J. J.Kelly, B. L. Berman, and D. J. Millener " Electron scattering from 9Be" *Phys. Rev*. C43, 1740, 1991.
[23] P.J. Brussaard and P. W. M. Glademans "*Shell- model Application in Nuclear Spectroscopy" North-Holland Publishing Company, Amsterdam*, 1977.
[24] B. A. Brown, B. H. Wildenthal, C. F. Williamson, F. N. Rad, S. Kowalski, Hall Crannell, and J. T. O'Brien " Shell-model analysis of high-resolution data for elastic and inelastic electron scattering on 19F" *Phys. Rev. C* 32, pp.1127-1156, 1985
[25] B. A. Brown, R. A. Radhi and B. H. Wildenthal "Electric Quadrupole and Hexadecupole Nuclear Excitations from the Perspectives Of Electron Scattering and Modern Shell-Model Theory" *Phys. Rep*. 101, No. 5, pp. 313-358. 1983.
[26] J. M. Finn, H. Crannel.L, P. L. Hallowsll and J. T. Obribn, "Inelastic Electron Scattering From Low-Lying States In The Nuclei 36Ar and 40Ar" *Nucl. Phys. A*290, pp.99-108, 1977.
[27] Archana Saxena and Praveen C. Srivastava "Ab initio no-core shell model study of 18−23O and 18−24F isotopes" *Phys. G: Nucl. Part. Phys*. 102959.R3, pp. 1-23, 2019.
[28] National Nuclear Data Center (NNDC), http://www.nndc. bnl.gov/.
[29] B. Pritychenkoa, M. Birchb, B. Singhb, M. Horoi, "Tables of E2 Transition Probabilities from the first 2+ States in Even-Even Nuclei", 2016.